Renewable Energy 252 (2025) 123547

Contents lists available at ScienceDirect

Renewable Energy

journal homepage: www.elsevier.com/locate/renene

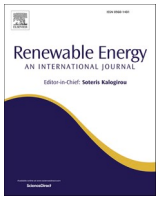

Dry torrefaction of biomass waste into high-energy biochar and selective formation of levoglucosenone and 1,4:3,6-dianhydro-α-D-glucopyranose

Andrii Kostyniuk *, Blaž Likozar

Department of Catalysis and Chemical Reaction Engineering, National Institute of Chemistry, Hajdrihova 19, Ljubljana, 1001, Slovenia

ARTICLE INFO

Keywords:
Dry torrefaction
Biomass waste
Wood cellulose pulp residue
Levoglucosenone
1,4:3,6-dianhydro-α-D-glucopyranose

ABSTRACT

For the first time, the non-catalytic formation of value-added liquid products, such as levoglucosenone (LGO) and 1,4:3,6-dianhydro-α-D-glucopyranose (DGP) from wood cellulose pulp residue (WCPR) has been achieved using dry torrefaction (DT) under solvent-free conditions and in a nitrogen atmosphere. This study systematically examined the influence of reaction conditions on the DT process, evaluating their effects on the surface morphology and elemental composition of the resulting biochar. This process encompassed a temperature range of 210–300 °C and reaction durations spanning from 15 to 60 min. Optimal conditions for liquid product selectivity were identified, achieving 67.7 % selectivity for LGO at 270 °C after 15 min and 32.6 % selectivity for DGP at 240 °C after 30 min. The highest yields were obtained at 300 °C after 60 min, reaching 10.5 % for LGO and 8.5 % for DGP. Various properties of the obtained biochar were thoroughly assessed, including the higher heating value (HHV), decarbonization, dehydrogenation, deoxygenation, enhancement factor, surface area, pore diameter, as well as solid, carbon, hydrogen, and energy yields. The highest carbon content, reaching 65.3 %, was achieved at 300 °C after 60 min of treatment, resulting in an HHV of 25.6 MJ/kg and an enhancement factor of 1.33. Finally, a comprehensive reaction pathway for the conversion of cellulose into LGO and DGP was proposed to elucidate the DT mechanism of WCPR. The results suggest that the autocatalytic nature of WCPR facilitates the selective formation of LGO and DGP through thermally induced dehydration and molecular rearrangement reactions, thereby enhancing the overall efficiency of biomass valorization.

1. Introduction

The increasing global population, industrialization, and growing fuel demand for transportation necessitate a shift toward renewable and alternative energy sources, as the reliance on fossil fuels remains the primary contributor to climate change, accounting for 80 % of greenhouse gas emissions in the European Union [1,2]. Biomass stands out as a leading renewable source of carbon, ranking as the fourth largest resource after coal, oil, and natural gas [3]. It presents an excellent alternative to traditional fossil fuels due to its abundance, renewability, carbon neutrality, and low pollution levels [1,4].

Thermochemical processing techniques, encompassing dry conversion methods like pyrolysis, dry torrefaction, and gasification, as well as wet conversion methods, are extensively employed to transform biomass into oil, char, and gas products [5,6]. Today, dry torrefaction (DT) is widely acknowledged as an effective pretreatment technique to address the inherent limitations of biomass fuel [7,8]. These limitations include low bulk density, high moisture content, suboptimal heating value, and low grindability. DT, a thermochemical conversion process ideal for dry biomass (less than 60 % moisture), operates at 200–300 °C for several minutes to hours in an oxygen-depleted (inert) atmosphere with atmospheric pressure, producing a solid product (biochar) with thermal and processing properties similar to coal with improved grindability and hydrophobicity, HHV, and energy density, making it suitable for replacing fossil fuels in combustion or gasification [9,10].

Lignocellulosic biomass, consisting of cellulose (40–50 %), hemicellulose (15–25 %) and lignin (15–30 %) is the most abundant source of carbon-based molecules [11]. Cellulose is a polydisperse linear polysaccharide composed of beta-1,4-glycosidic linked D-glucose units, known as anhydroglucose units. It can be depolymerized to produce anhydrosugars through pyrolysis or dehydration under anhydrous conditions [12,13]. Cellulose can be converted into a variety of chemical platforms, including glucose, furfural, 5-hydroxymethyl furfural (5-HMF), 2,5-furandicarboxylic acid, 2,5-diformylfuran, 2,5-dimethylfuran, lactic acid, acetic acid, levulinic acid, γ-valerolactone, ethanol, itaconic acid, levoglucosan (LGA), etc. [14,15]. Another

* Corresponding author.
E-mail address: andrii.kostyniuk@ki.si (A. Kostyniuk).

https://doi.org/10.1016/j.renene.2025.123547
Received 16 February 2025; Received in revised form 14 May 2025; Accepted 21 May 2025
Available online 22 May 2025

anhydrosugar that can be selectively derived from cellulose through dehydration, pyrolysis, or catalytic processes is levoglucosenone (1, 6-anhydro-3,4-dideoxy-beta-D-glycero-hex-3-enopyran-2-ulose, LGO) features a double bond conjugated with a ketone, along with a protected aldehyde and two protected hydroxyl groups [16]. LGO was recently recognized as one of the top 10 platform chemicals [17]. LGO holds a distinct advantage over other biomass-derived platform chemicals due to its ability to be directly produced through the pyrolysis of cellulose-containing materials, including waste products like discarded paper. However, a significant drawback is that LGO yields remain consistently low, typically less than 3 wt%, regardless of the specific operating conditions or type of feedstock used [18].

At the same time, producing LGO from non-sugar compounds through chemical synthesis is constrained by lengthy synthesis procedures and intricate reactions [19]. LGO unique structure and potential as a chiral building block have made it an attractive platform molecule, valued for producing solvents, polymers, and scaffolds for drug discovery, with its derivatives demonstrating anticancer, antitumor, and antimicrobial activities [20,21]. LGO is produced at a rate of 50 T per year, with production set to increase to 1000 T per year soon [22]. Moreover, the current high cost of LGO (in the range of 470–1000 USD/g) limits the ability to thoroughly assess its full potential as a biorenewable platform chemical [23]. To make LGO more accessible, it is essential to develop a method that enables its efficient production in high yield [18]. 1,4:3,6-Dianhydro-α-D-glucopyranose (DGP) is another unique anhydrosugar with a rigid, multicyclic chiral structure, no unsaturated C=O and C=C bonds, but possessing a hydroxyl group, making it valuable in chemical synthesis [24,25]. Despite its potential as a versatile starting material in both carbohydrate chemistry and the synthesis of non-carbohydrate and non-natural compounds, the conventional chemical synthesis of DGP is challenging and costly, leading to limited market availability and rare applications; alternatively, DGP can be produced through the fast pyrolysis of cellulose, though with low yield [24].

In this study, a novel, sustainable method for the DT of wood cellulose pulp residue (WCPR) was developed using a horizontal tubular quartz reactor in a nitrogen atmosphere. For the first time, selective production of LGO and DGP from WCPR without a catalyst was achieved. The effects of DT temperature and time were examined. The primary goal of this research was to enhance the production of biochar with higher HHVs and increased carbon content, while also generating valuable liquid products such as LGO and DGP. Comprehensive characterization of both WCPR and the biochar produced after the DT process was conducted using various techniques, including Brunauer-Emmett-Teller (BET) analysis, scanning electron microscopy (SEM), X-ray diffraction (XRD), CHN(O)S elemental analysis, and thermogravimetric analysis (TGA). These analyses provided valuable insights into the structural and compositional properties of the biochar. The structures of LGO and DGP were confirmed by gas chromatography/mass spectrometry (GC/MS). Furthermore, the formation mechanisms of LGO and DGP were proposed and analyzed in detail.

This work supports sustainable energy development by transforming renewable biomass into energy-dense solid fuels and valuable chemical intermediates. The biochar produced under optimized DT conditions exhibited a significantly improved HHV of up to 25.6 MJ/kg, making it a viable renewable alternative to fossil coal in energy production systems. In addition, the selective formation of platform chemicals such as LGO and DGP adds a further dimension to biomass valorization. These compounds serve as biorenewable platform chemicals, supporting the integrated biorefinery concept that underpins many renewable energy strategies. Their potential conversion into fuels and green chemicals contributes to a circular, fossil-independent energy economy. Importantly, our process operates under solvent-free, non-catalytic conditions in an inert atmosphere, offering a more energy-efficient and scalable route for renewable energy and chemical production. Therefore, this work contributes to renewable energy research by advancing biomass-based fuel production, improving energy density of renewable solids, and generating chemical intermediates that can reduce dependence on fossil resources.

2. Experimental section

Detailed information on materials, analysis, and calculations is available in the Supporting **Information file** (ESI) including the composition of WCPR feedstock (Table S1).

2.1. Experimental apparatus and procedure

Before using WCPR for DT, the feedstock was dried at 40–45 °C overnight. Approximately 5.0 g of the WCPR sample was accurately weighed and placed into a quartz glass boat, which was then sealed inside a horizontal tubular quartz reactor with a three-zone electric furnace. The WCPR underwent DT in a nitrogen atmosphere at a flow rate of 200 mL/min (Fig. 1). After DT, the quartz glass boat was reweighed to determine the mass loss. The organic liquid products generated during the DT process were collected from the condenser, filtered, and analyzed using gas chromatography-mass spectrometry (GC-MS). Highly volatile compounds were absorbed in a second water-filled condenser, while non-absorbed gaseous products were directed to a micro-GC for analysis. The analysis of liquid products was conducted using an Agilent GC-7890A coupled with an Agilent 5977B GC/MSD, equipped with a DB-WAX Ultra Inert capillary column (30 m length, 0.25 mm internal diameter, 0.25 μm film thickness), with external calibration used for identification and quantification.

For optimal separation of the products, the column temperature was initially held at 40 °C for 4 min, then increased to 230 °C at a rate of 15 °C/min, and held at this final temperature for 12 min. The split ratio was set at 1:30, with a total flow rate of 34.5 mL/min, resulting in a total runtime of 32 min. The experiments examined four torrefaction temperatures (210, 240, 270, and 300 °C), representing light, mild, and severe torrefaction, with durations of 15, 30, and 60 min.

The experiments were conducted in triplicate with deviations below 5 %, and the product compounds were identified using the NIST MS spectral database (Fig. S1). Gas composition analysis was conducted using an Agilent 490 Micro GC equipped with thermal conductivity detectors (TCD) and CP-Molsieve and PoraPlot U columns. Across all samples, the detected concentrations were as follows: N_2 (50.4–50.6 %), CO_2 (28.8–29.8 %), CO (13.2–14.1 %), H_2 (3.2–5.3 %), and C_2-C_4 hydrocarbons (ethane, propane/propylene, and butane) at 1.6 %.

Wet torrefaction (WT) reactions of WCPR were conducted in six stainless steel, 75 mL batch reactors, each equipped with pressure and temperature control regulators, and heated at a rate of 10 °C/min [26,27]. The reaction mixture was stirred at 800 rpm using a magnetic stirring bar, with 3.0 g of WCPR introduced into each reactor. Temperature control was managed by an electric heating system, with inline thermocouples monitoring the internal temperature. Once the target reaction temperature was reached, the reaction time commenced, and after completion, the reactors were rapidly cooled in an ice bath. Hydrochars were separated from the liquid products by filtration, dried at 105 °C for 24 h, and stored in a desiccator with silica gel, while product solutions were collected using a 0.22 μm membrane filter.

3. Results and discussion

3.1. Effect of reaction time and temperature on the product selectivity and yield in the liquid phase after DT of WCPR

In this study, the impact of reaction time and temperature on the product distribution during the conversion of WCPR was investigated (Fig. 2). The experimental conditions were standardized with a constant amount of 5.0 g of WCPR, a N_2 flow rate of 200 mL/min, and a reaction temperature range from 210 to 300 °C. The reaction times were varied

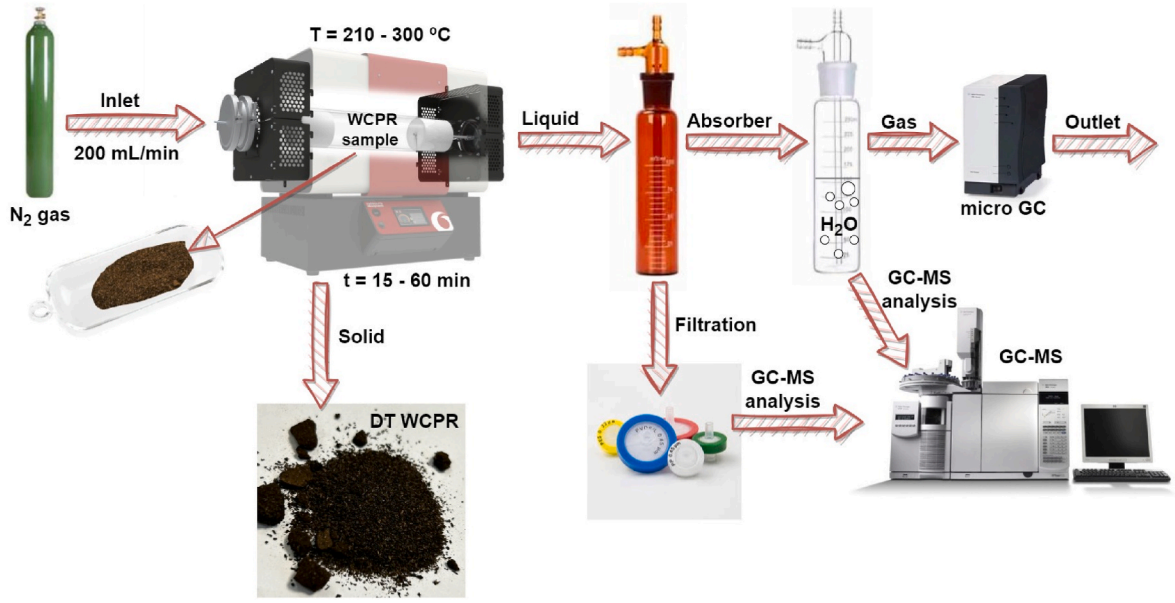

Fig. 1. Schematic view of horizontal reactor, furnace, and equipment utilized for DT of WCPR.

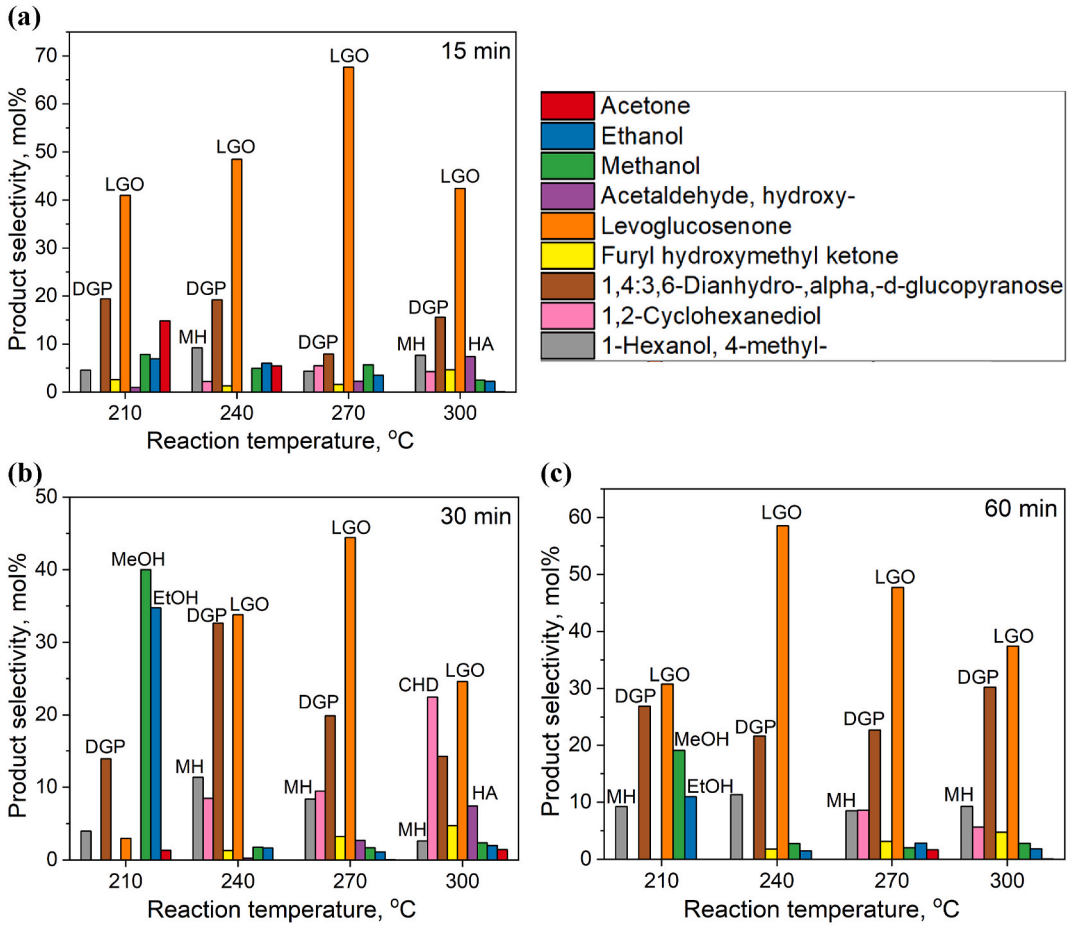

Fig. 2. Effect of reaction time (a – 15 min, b – 30 min, c – 60 min) and temperature on the liquid-phase product selectivity in the DT of WCPR. Reaction conditions: 5.0 g of WCPR, N_2 flow of 200 mL/min, reaction temperature ranging from 210 to 300 °C, and reaction time from 15 to 60 min. Abbreviations: LGO – levoglucosenone, DGP – 1,4:3,6-dianhydro-α-D-glucopyranose, MH – 4-methyl-1-hexanol, CHD – 1,2-cyclohexanediol, HA – hydroxyacetaldehyde. Other detected products in low concentrations include: 5-HMF; 5-methylfurfural; furfural; acetic acid; hydroxyacetone; levulinic acid; formaldehyde; cyclopentenone; 3-methyl-1,2-cyclopentanedione; furaneol; trans-1,3-cyclohexanediol.

between 15 and 60 min, allowing for a comprehensive analysis of the product distribution at different stages of the reaction. At the initial 15 min mark, the product distribution reveals the early stages of cellulose breakdown. The presence of both DGP and LGO indicates that cellulose is beginning to decompose, likely through pyrolytic processes. While DGP is present initially, its amount decreases as more LGO is formed. HA is also detected, suggesting the formation of smaller aldehyde compounds. At this stage, while other compounds may be forming, they are not yet predominant.

This observation underscores the importance of early reaction dynamics in shaping subsequent product profiles. As the reaction time extends to 30 min, the product profile evolves. LGO remains a significant component, reflecting its ongoing formation and stability. Notably, DGP begins to emerge, indicating secondary reactions that lead to more complex anhydrosugars. The appearance of MH suggests further transformation of initial breakdown products into alcohols. At 60 min, the product distribution becomes more complex. LGO continues to dominate, reinforcing its role as a key intermediate or final product in this process. The presence of DGP becomes more pronounced, indicating that longer reaction times favor its formation. The emergence of MH and CHD points to further secondary reactions and the formation of more diverse alcohol products. Temperature is a crucial factor in determining the product distribution. Higher temperatures within the range of 210–300 °C likely accelerate the breakdown of cellulose and the formation of secondary products. The stability of LGO across different temperatures indicates its robustness as a product (Fig. 2a).

LGO is known to form primarily through a fast, thermally driven dehydration of cellulose intermediates, such as LGA, under mild pyrolytic conditions. Our results indicate that 270 °C provides an optimal balance between reaction temperature and energy input, enabling the selective formation of LGO while minimizing its secondary degradation. At this temperature, the breakdown of cellulose is sufficiently activated to generate LGO in high yield, yet harsh cracking or overreaction pathways are not yet dominant. This explains the peak LGO selectivity (67.7 %) observed at 270 °C after 15 min.

In contrast, DGP appears to accumulate more significantly at longer residence times (30–60 min), particularly at moderately elevated temperatures (240–270 °C). This behavior is attributed to the fact that DGP formation involves slower intramolecular dehydration and ring-closure reactions, likely proceeding via intermediate anhydrosugars. These reactions require more time to reach completion and are favored under relatively stable thermal conditions where secondary transformations can occur. Therefore, extended residence times facilitate DGP accumulation, while LGO remains dominant at early stages due to its rapid formation and thermal stability.

Fig. 3 illustrates the effect of reaction temperature and residence time on the yields of the main products – LGO and DGP. As shown in Fig. 3a, the LGO yield increases with temperature, suggesting that higher temperatures promote its formation through the dehydration and rearrangement of cellulose-derived intermediates. For a reaction time of 15 min, the LGO yield progressively rises, reaching 10.3 % at 300 °C. A similar trend is observed for 30 min, but with a lower maximum yield of 7.1 %, suggesting partial degradation at extended exposure.

Notably, at 60 min, the LGO yield reaches its highest value of 10.5 % at 300 °C, demonstrating that prolonged heating enhances the conversion of WCPR into LGO. However, at 30 min and 300 °C, a noticeable drop in LGO yield is observed compared to the shorter and longer residence times, likely due to secondary degradation reactions, such as overcracking into volatile products or polymerization into char. This indicates that while high temperatures facilitate LGO formation, excessive exposure (>270 °C) can lead to decomposition, underscoring the need for temperature-time optimization to maximize LGO yield while minimizing degradation.

Unlike LGO, DGP formation follows a different pattern, as shown in Fig. 3b. At 210–240 °C, the DGP yield remains low, suggesting that its formation is thermally less favorable and requires higher temperatures to proceed efficiently. For 15 and 30 min, the yield remains below 4 % at all temperatures, implying minimal formation. However, at 60 min, the yield gradually increases, reaching 8.5 % at 300 °C, indicating that prolonged heating promotes its formation, possibly via sequential dehydration and rearrangement reactions. The low DGP yield at 15 min across all temperatures implies that its formation pathway may require prolonged thermal exposure, likely involving intermediate fragmentation and anhydrosugar reorganization. The significant increase in DGP yield at 60 min and 300 °C suggests that it forms as a secondary product, favored by progressive dehydration and cyclization reactions. The residence time plays a crucial role in determining the product distribution. While prolonged reaction times favor the conversion of WCPR-derived intermediates into both LGO and DGP, excessive heating leads to LGO degradation while enhancing DGP formation. This indicates that LGO formation is optimized at moderate temperatures and shorter reaction times, whereas DGP formation benefits from extended heating at higher temperatures.

Fig. S2 presented compare the product distribution in mol% for the decomposition of WCPR under DT and WT. Both reactions were conducted at 260 °C for 30 min, but the DT process involved a N_2 flow of 200 mL/min with 5.0 g of WCPR, while the WT process involved 3.0 g of WCPR in 30 mL of water with a stirring speed of 900 rpm in N_2 atmosphere, as detailed in our recent study [27].

The product distribution in the DT process is dominated by LGO,

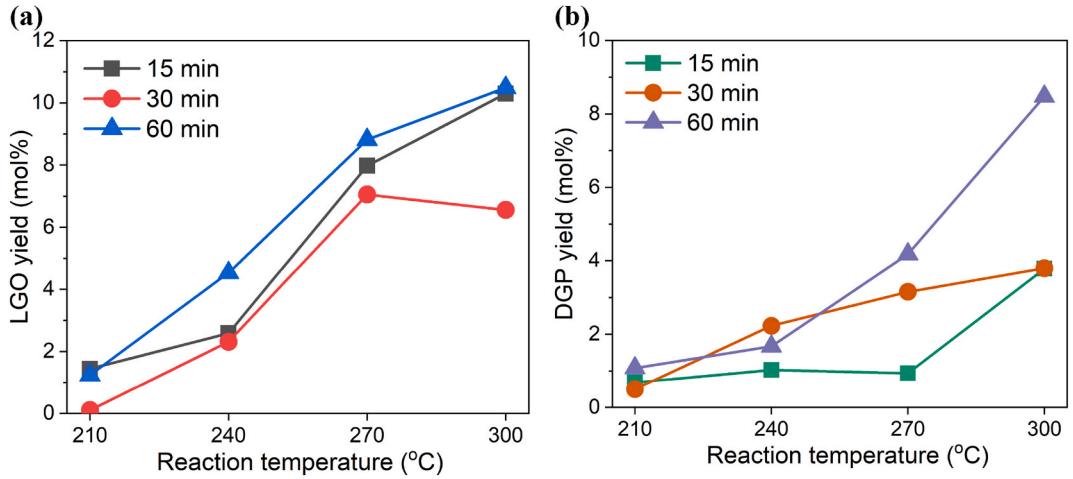

Fig. 3. Effect of reaction temperature and time on yields of LGO – (a) and DGP – (b). Reaction conditions: 5.0 g of WCPR, N_2 flow of 200 mL/min, reaction temperature ranging from 210 to 300 °C, and a reaction time of 15–60 min.

which accounts more than 60 % among the detected products (Fig. S2a). This indicates that under dry conditions, LGO is the major product formed from the decomposition of cellulose. In contrast, the WT process produces a more diverse array of compounds, with no single product dominating the distribution (Fig. S2b). This diversity suggests that the presence of water, the high stirring speed and pressure promote a different set of reactions, leading to the formation of various furan derivatives, ketones, acids, and alcohols. The presence of furfural, acetic acid, and levulinic acid indicates that hydrolysis and dehydration reactions are significant under WT conditions.

3.2. Effect of reaction temperature and time on conversion and solid yield of WCPR

The conversion of WCPR is strongly influenced by both reaction temperature and reaction time, as evidenced by the data presented in Fig. 4a and Table S3. At the lower end of the temperature range (210 °C), the conversion of WCPR remains minimal, with percentages barely exceeding 5 % even after 60 min. This suggests that 210 °C is insufficient to overcome the activation energy barriers necessary for significant cellulose decomposition. As the temperature increases to 240 °C, there is a noticeable rise in conversion rates (8.6–12.4 %), particularly for the longer reaction times of 30 and 60 min. This indicates that higher temperatures facilitate the breakdown of cellulose into smaller molecules, initiating more substantial thermal degradation processes. At 270 °C, the conversion rates exhibit a marked increase, with the 60 min reaction time achieving conversion rates close to 30 %. This temperature appears to be critical for initiating extensive decomposition of cellulose, highlighting its potential as an optimal point for effective cellulose conversion into LGO.

The highest conversion rates are observed at 300 °C, where the 60 min reaction time results in 45.0 % conversion. This significant increase underscores the role of higher temperatures in enhancing the thermal degradation of cellulose. The solid yield data presented in Fig. 4b and Table S3 provide complementary insights into the decomposition process. At 210 °C, the solid yield remains high, around 94–95 % for all reaction times, reinforcing the observation that this temperature is not sufficient for substantial cellulose breakdown. A notable decrease in solid yield is observed as the temperature increases to 240 °C, especially at longer reaction times. This decrease correlates with the increased conversion rates, indicating that more cellulose is being converted into liquid and gaseous products, thus reducing the residual solid fraction. At 270 °C, the solid yield drops significantly, with the 60 min reaction time resulting in a yield of around 70 %. The trend continues at 300 °C, where the solid yield further decreases to 55.0 % for the 60 min reaction time. This indicates extensive decomposition and conversion of cellulose, with only a small fraction remaining as solid residue.

3.3. TG analysis of WCPR and DT WCPR samples

The thermogravimetric (TG) curves in Fig. 5 illustrate the thermal degradation behavior of WCPR and its DT product (biochar) at different temperatures and reaction times. The samples were heated from 20 to 800 °C at a rate of 10 °C/min in a N_2 atmosphere. For the samples torrefied at 210 °C, the residual weights are: 15 min–20.0 %, 30 min–20.6 %, 60 min–18.3 %.

These values indicate that the thermal degradation at 210 °C is relatively low, with the residual weights remaining close to the WCPR feedstock's residual weight of 18.3 %. The slight variations in residual weight with time suggest minimal additional decomposition occurring at this temperature. At 240 °C, the residual weights are similar to those at 210 °C: 15 min–20.0 %, 30 min–20.6 %, 60 min–21.3 %. The samples treated at 270 °C show an increase in residual weights: 15 min–25.8 %, 30 min–30.6 %, 60 min–33.0 %. This increase in residual weights at higher torrefaction temperature suggests the formation of more thermally stable products – biochar or other byproducts resistant to further degradation. At 300 °C, the residual weights are significantly higher: 15 min–40.4 %, 30 min–44.9 %, 60 min–48.6 %. These results indicate the highest formation of stable residues at 300 °C. The substantial increase in residual weights with temperature suggests that extensive thermal degradation occurs, resulting in the formation of thermally stable biochar.

3.4. HR SEM analysis of WCPR and DT WCPR samples

The scanning electron microscopy (SEM) images of WCPR and its DT sample at 300 °C for 60 min reveal significant morphological changes, reflecting the impact of high-temperature torrefaction on the material microstructure (Fig. 6). The SEM image of the untreated WCPR (Fig. 6a–c) shows a fibrous and layered structure typical of cellulose-based biomass. The fibers are closely packed, and the overall structure appears relatively intact, with minimal signs of degradation or structural collapse. The presence of these fibers indicates the high degree of polymerization and structural integrity of the cellulose in its natural state. In contrast, the SEM image of the DT WCPR sample (Fig. 6b–d) exhibits a markedly different morphology. The sample treated at 300 °C for 60 min was selected for SEM analysis, as this condition represents the most intensive torrefaction scenario investigated. Under these conditions, the biomass exhibited the highest carbon content and the most pronounced morphological changes. This allowed for a more detailed

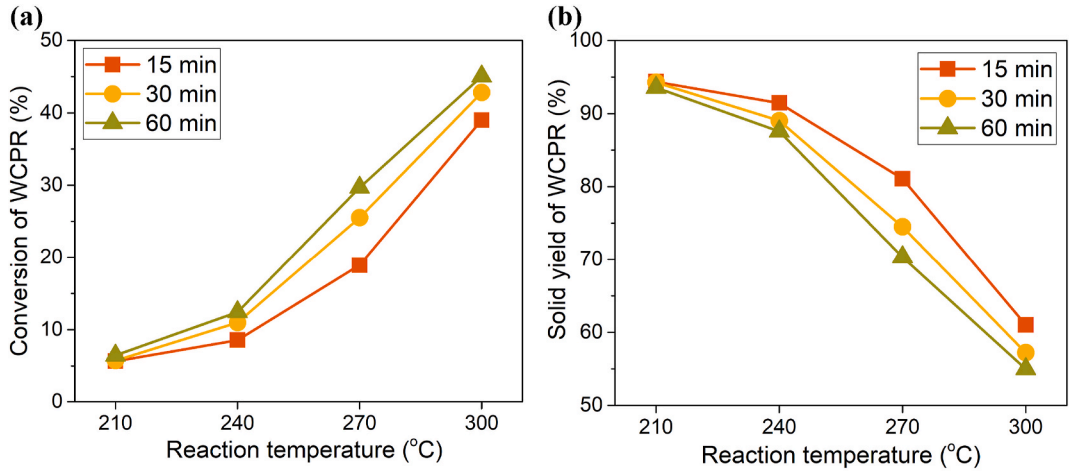

Fig. 4. Effect of reaction temperature and time on conversion of WCPR – (a) and its solid yield – (b). Reaction conditions: 5.0 g of WCPR, N_2 flow of 200 mL/min, reaction temperature ranging from 210 to 300 °C, and a reaction time of 15–60 min.

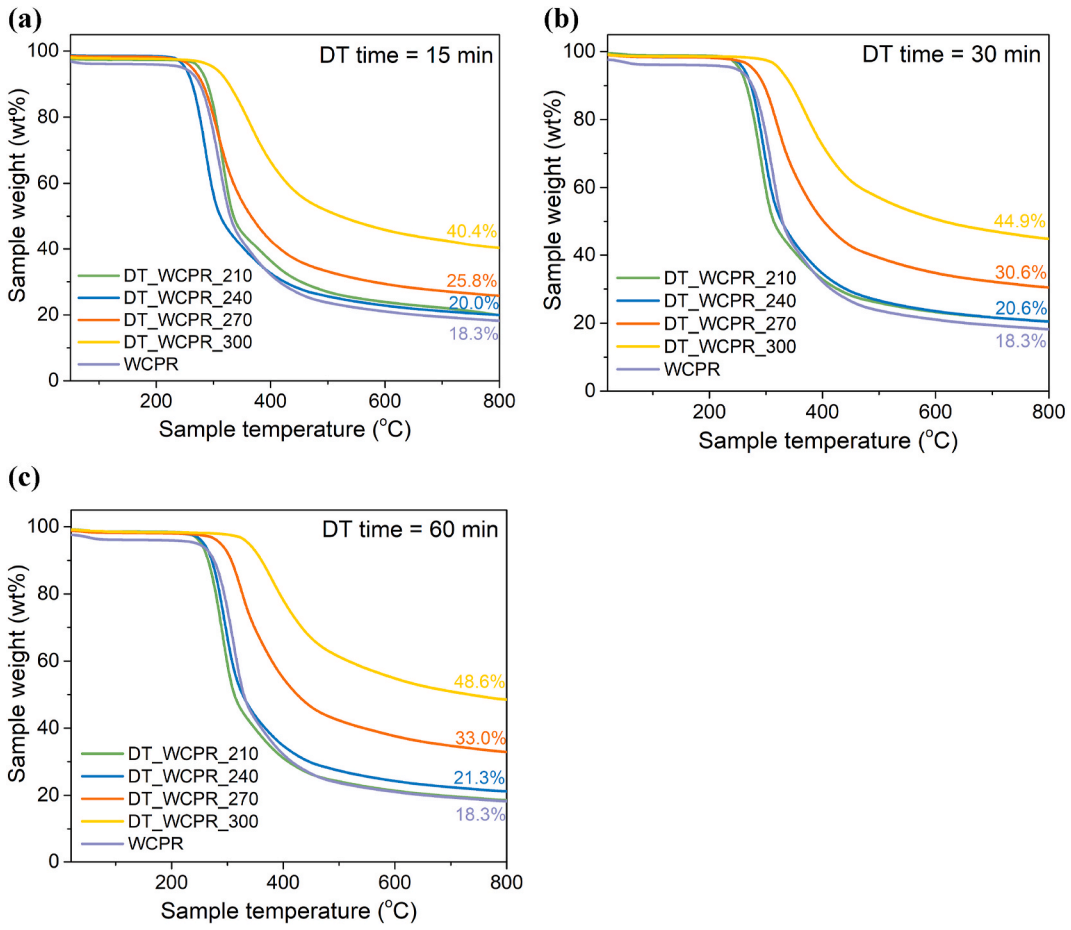

Fig. 5. TG curves of WCPR and DT of WCPR in the temperature range of 20–800 °C at 15 min – (a), 30 min – (b), and 60 min – (c) with heating rate of 10 °C/min in nitrogen atmosphere.

observation of the structural transformation of WCPR during DT.

The fibrous structure observed in the untreated WCPR has been substantially altered. The DT-treated sample shows a highly porous structure with significant voids and cavities. This increase in porosity is indicative of the extensive thermal degradation and volatilization of organic components, leading to the formation of biochar with a more open and porous structure. This structural transformation is further confirmed by N_2 adsorption-desorption experiments (Table S2), which show an increase in the pore diameter from 73 Å in the untreated WCPR to 215 Å in the DT WCPR sample at 300 °C. This increase in porosity is indicative of the extensive thermal degradation and volatilization of organic components, leading to the formation of biochar with a more open and porous structure. The layered structure of the original WCPR has collapsed, forming a more irregular and fragmented morphology. This collapse is likely due to the breakdown of cellulose and hemicellulose components, which lose their integrity at high temperatures.

3.5. XRD analysis of WCPR and DT WCPR samples

The XRD patterns of WCPR and DT WCPR at different temperatures (210–300 °C) and durations (15, 30, and 60 min) reveal important insights into the structural transformations and crystallinity changes induced by dry torrefaction. The XRD patterns in Fig. 7 illustrate the key diffraction peaks corresponding to the crystalline planes of cellulose I, specifically at 2θ values of approximately 15.6° (110), 22.4° (200), and 34.4° (004). The XRD pattern of untreated WCPR shows well-defined peaks at 15.6°, 22.4°, and 34.4°, indicating a high degree of crystallinity typical of cellulose I structure. The intensity of these peaks signifies the presence of ordered crystalline regions within the biomass waste. The samples treated at 210 and 240 °C for different durations exhibit minor reductions in peak intensities compared to untreated WCPR.

This suggests that low-temperature torrefaction induces slight degradation of the cellulose crystalline structure, but a significant amount of crystallinity is retained. The residual weights of these samples, as indicated by TGA, are also similar to those of untreated WCPR, further confirming the limited structural degradation at these temperatures. At 270 °C, there is a noticeable reduction in the intensity of the crystalline peaks. The peaks at 15.6° and 22.4° become broader and less defined, indicating partial disruption of the crystalline cellulose structure.

The XRD patterns of samples treated at 300 °C for different durations show significant broadening and reduction in the intensity of the characteristic cellulose peaks. This indicates extensive degradation of the crystalline regions, leading to a more amorphous structure. The most significant structural changes occur at 60 min, with 300 °C samples showing almost complete loss of distinct crystalline peaks. This suggests that prolonged exposure to high temperatures leads to extensive amorphization and formation of a stable biochar structure. The impact of DT duration and temperature on the crystallinity index and crystallite size of WCPR was investigated after XRD analysis. Fig. 7d and e provide valuable insights into the structural evolution of the WCPR samples subjected to different thermal treatments. The data in Fig. 7d and Table S2 reveal a consistent trend of decreasing crystallinity with increasing temperature and time of treatment. At 210 °C, a significant reduction in crystallinity is observed, with values dropping from 76.5 % in untreated WCPR to around 71.2–73.5 % for all treatment durations. Further temperature increase to 240 °C results in a more pronounced

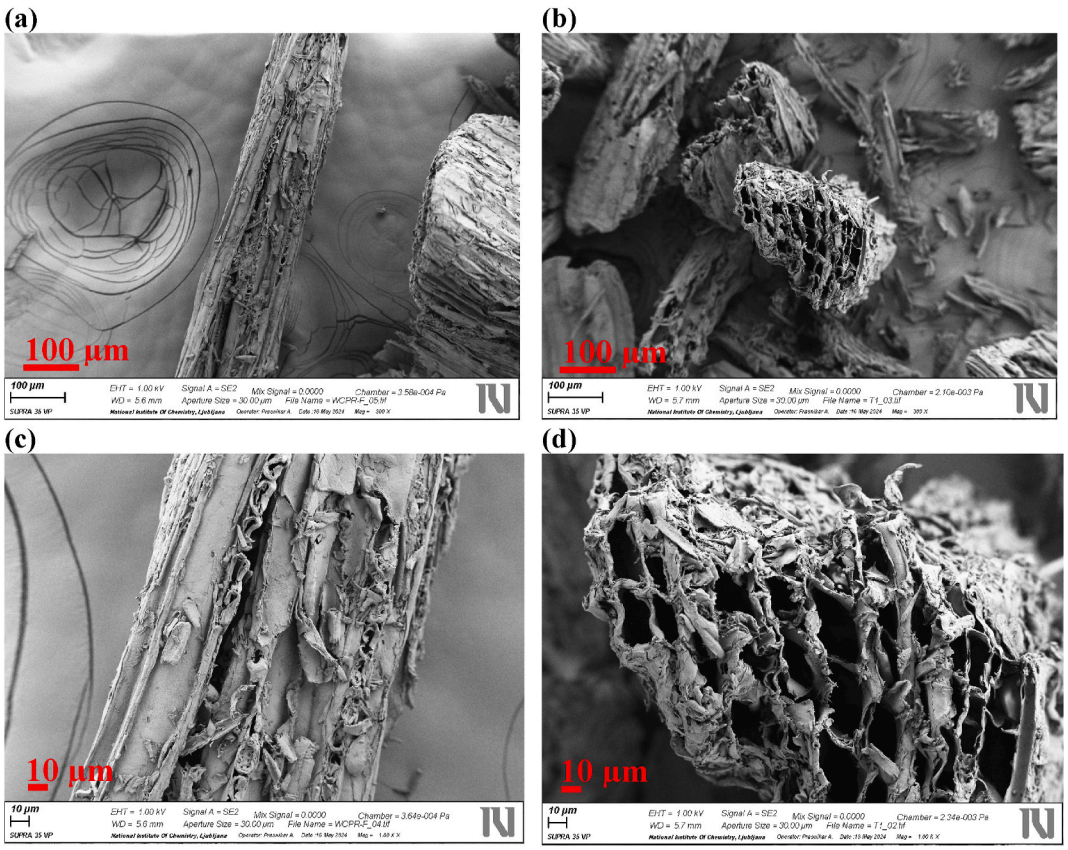

Fig. 6. SEM images of untreated WCPR (a, c) and DT-treated WCPR (b, d) after treatment at 300 °C for 60 min. Images (a) and (b) include 100 µm scale bars at 300× magnification, while images (c) and (d) include 10 µm scale bars at 1.00 kX magnification.

decline, with crystallinity indices falling to 61.4–69.5 %. At 270 °C, the crystallinity index continues to decrease, reaching values close to 28.0–48.1 %. The most drastic reduction is seen at 300 °C, where the crystallinity index plummets to around 6.7–10.7 %, indicating substantial amorphization of the cellulose structure. Interestingly, the duration of heat treatment appears to have a less significant effect on the crystallinity index compared to the temperature. This suggests that temperature is the dominant factor influencing the structural changes in the WCPR samples during DT.

Fig. 7e and Table S2 show the variation in crystallite size for the same set of WCPR samples. The trend is similar to that observed for the crystallinity index, with crystallite size decreasing as temperature and duration of heat treatment increase. The untreated WCPR samples exhibit an average crystallite size of 3.3 nm. At 210 °C, the crystallite size slightly decreases to 3.1–3.2 nm, with minimal differences among the different durations of heat treatment. At 240 °C, a more noticeable reduction in crystallite size is evident, with values dropping to around 2.5–3.0 nm. The crystallite size continues to decline with increasing temperature, reaching 1.0–1.1 nm at 270 °C. At the highest temperature of 300 °C, the crystallite size reaches its minimum, ranging from 0.7 to 0.8 nm. Similar to the crystallinity index, the temperature plays a crucial role in determining the crystallite size, with the duration of treatment having a secondary effect.

3.6. Elemental components and surface properties of WCPR and DT WCPR samples

Table S2 presents a comprehensive analysis of the proximate and elemental composition, along with the BET surface area and average pore diameter (PD) of WCPR and its DT samples at various reaction temperatures and times. The moisture content in the untreated WCPR is 3.9 %, which decreases significantly after DT treatment. The volatile matter (VM) content shows a slight decrease with increasing temperature and time. The DT_WCPR_300 (60 min) sample exhibits the lowest VM at 51.8 %, compared to the untreated WCPR at 78.7 %. Fixed carbon (FC) content increases with higher temperatures and longer durations of torrefaction, with DT_WCPR_300 (60 min) showing the highest FC content of 40.9 %. This trend indicates that higher temperatures and longer treatment times enhance the carbonization process, resulting in higher FC content and lower VM.

Carbon (C) content increases significantly with higher torrefaction temperatures and longer durations (Table S2). The untreated WCPR has a carbon content of 48.3 %, which rises to 65.3 % in DT_WCPR_300 (60 min). This increase in carbon content corresponds with a decrease in oxygen (O) content, indicating a progressive deoxygenation process during torrefaction. Hydrogen (H) and nitrogen (N) contents show minor fluctuations across the samples, with no consistent trend observed. Sulfur (S) content remains relatively low across all samples, with a slight increase at higher torrefaction temperatures. The BET surface area of the untreated WCPR is 3.4 m^2/g. After DT, the surface area shows varied changes. The highest surface area is observed in DT_WCPR_240 (60 min) with 4.4 m^2/g, while the lowest is in DT_WCPR_300 (30 min) with 2.5 m^2/g. These variations suggest that DT conditions significantly affect the surface area, potentially due to changes in the material's porosity and structure. The average PD increases with higher DT temperatures and longer durations, reaching a maximum of 726 Å in DT_WCPR_300 (30 min). The results indicate that DT effectively reduces moisture and VM while increasing FC content and carbon concentration in WCPR. These changes enhance the material's energy density and stability, making it more suitable for applications like bioenergy production. The variations in BET surface area and PD suggest that optimizing DT conditions can tailor the material's

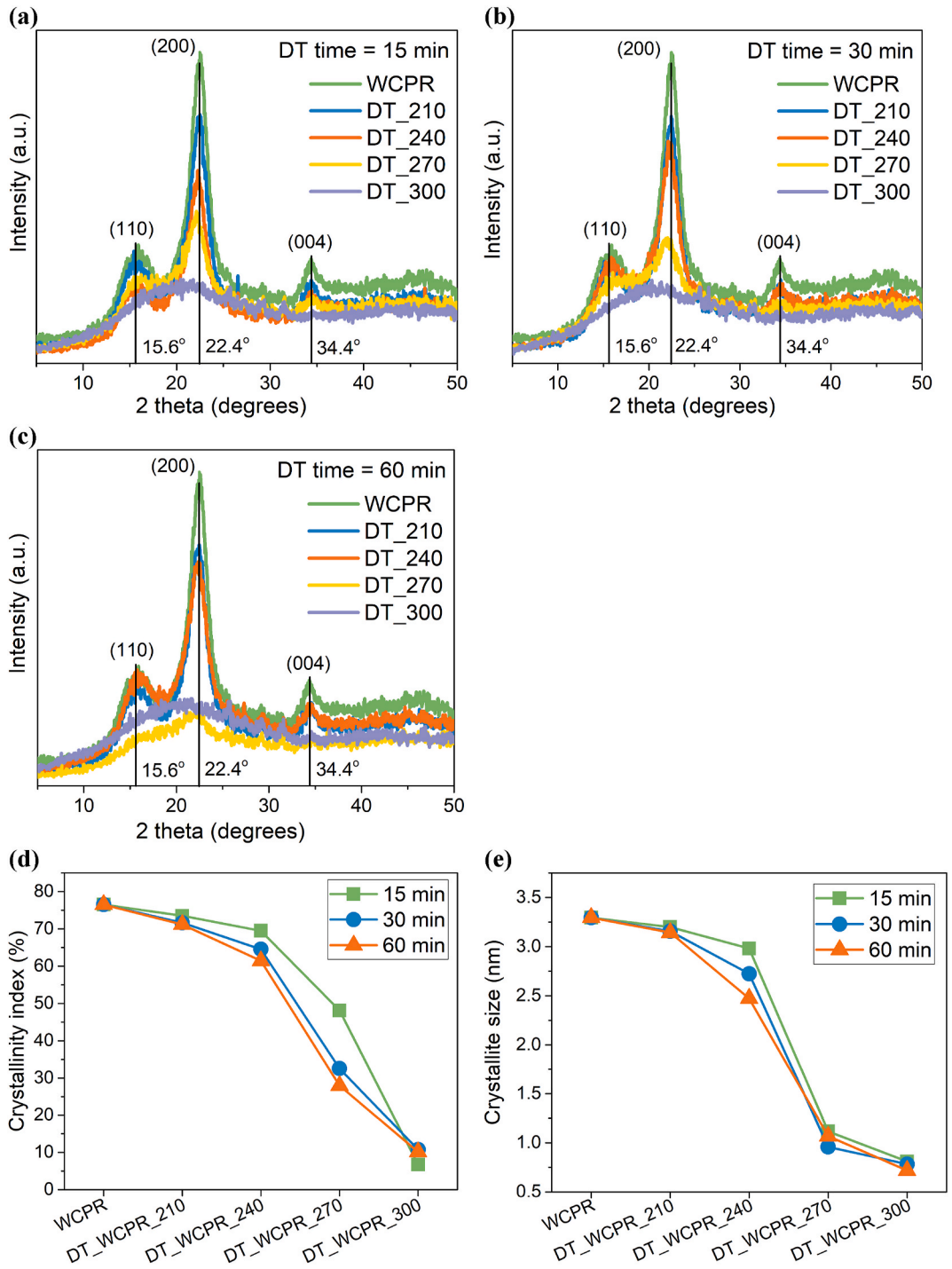

Fig. 7. Comparison of X-ray diffraction patterns of the DT of WCPR samples at temperatures ranging from 210 to 300 °C (DT_210 – DT_300) with WCPR samples subjected to different durations of heat treatment: 15 min – (a), 30 min – (b), and 60 min – (c). Additionally, analysis includes crystallinity index – (d) and crystallite size – (e).

properties for specific applications, such as adsorption or catalysis.

3.7. HHV, solid, carbon, hydrogen, energy yields, DC, DH, DO, ARE, enhancement factor and atomic ratios of O/C and H/C of WCPR and DT WCPR samples

The effect of heat treatment duration and temperature on the higher heating value (HHV) and energy yield of WCPR is presented in Fig. 8. These parameters are crucial for assessing the energy potential of WCPR when subjected to thermal treatments. Fig. 8a demonstrates the HHV of WCPR samples treated at various temperatures for different durations. The results show a clear trend of increasing HHV with rising temperature and duration of heat treatment. The untreated WCPR sample has an HHV of approximately 19 MJ/kg. At 210 °C, the HHV shows a slight increase to around 20.0–20.1 MJ/kg, with the values for 15, 30, and 60 min being closely aligned. As the temperature increases to 240 °C, the HHV further increases, reaching approximately 20.4 MJ/kg. A more significant increase is observed at 270 °C, where the HHV rises to around 21.2–22.9 MJ/kg. The highest HHV values are recorded at 300 °C, where the HHV reaches approximately 24.6–25.6 MJ/kg, with the 60

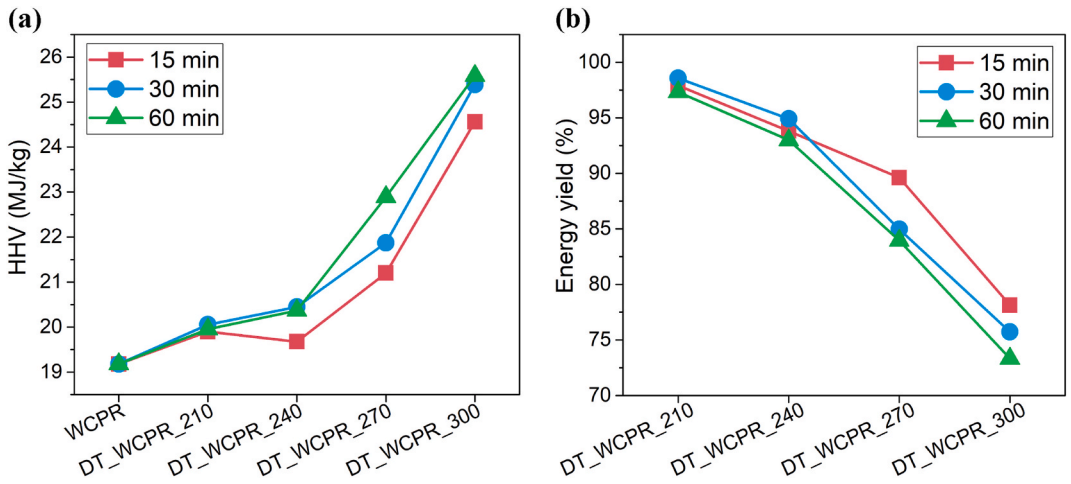

Fig. 8. HHV – (a) and energy yield – (b) for different durations (15–60 min) of WCPR and DT WCPR samples.

min treatment showing the highest value. The increase in HHV with temperature and duration indicates enhanced energy content in the DT WCPR, making it a more efficient fuel source. The prolonged duration of treatment at higher temperatures contributes to more extensive thermal degradation, leading to higher HHV values.

Fig. 8b and Table S3 show the energy yield of WCPR samples. Energy yield is a measure of the efficiency of the thermal treatment in conserving the energy content of the original material. At 210 °C, the energy yield decreases slightly to around 97–99 %, with minimal variation between different durations. As the temperature increases to 240 °C, the energy yield declines further to approximately 93–95 %. At 270 °C, a more pronounced reduction in energy yield is observed, with values dropping to around 84–90 %. The most significant decrease in energy yield occurs at 300 °C, where it falls to approximately 73–78 %, with the 60 min treatment resulting in the lowest yield at around 73.3 %. The decline in energy yield with increasing temperature and duration suggests that while the thermal treatment enhances the HHV, it also leads to greater loss of solid yield. This trade-off indicates that

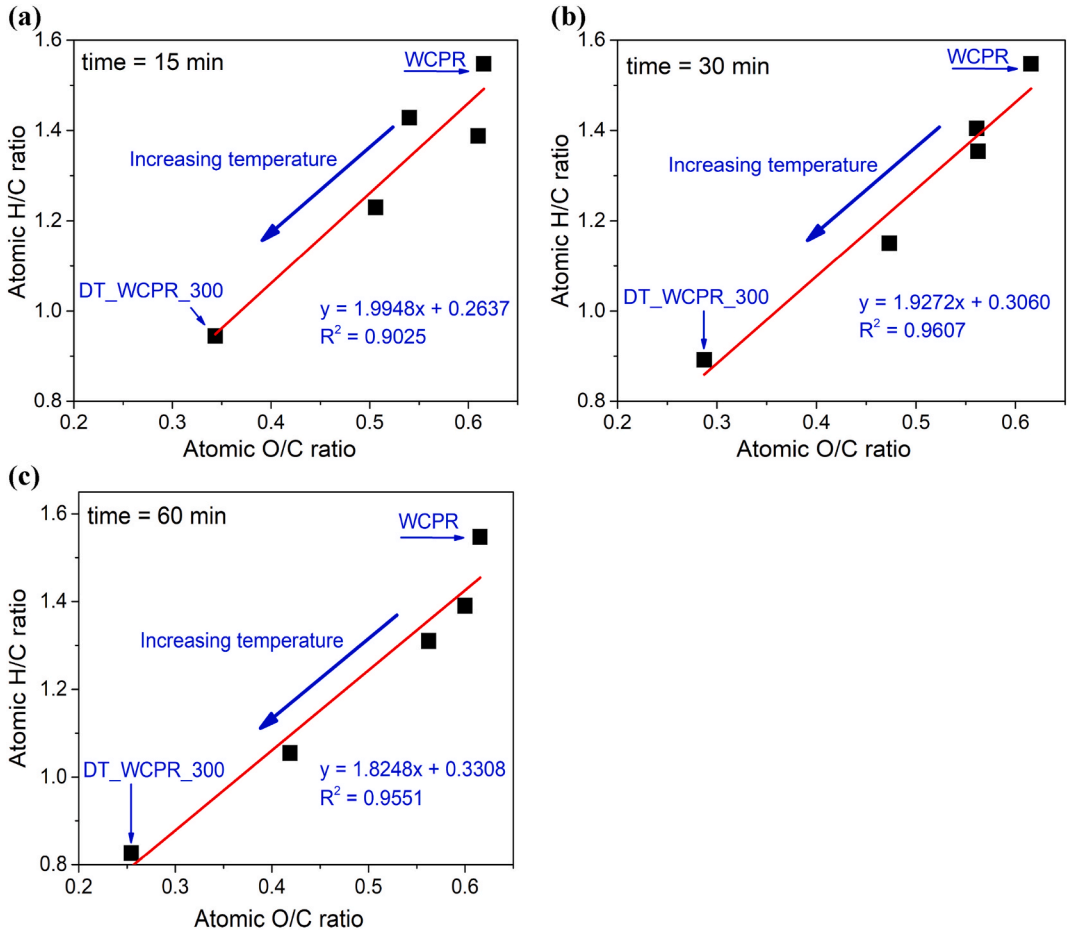

Fig. 9. H/C versus O/C ratio in terms of atomic basis (van Krevelen diagram) for different durations of DT of WCPR: 15 min – (a), 30 min – (b), and 60 min – (c).

optimizing the dry torrefaction conditions is essential to balance between maximizing HHV and minimizing energy losses.

The van Krevelen diagrams in Fig. 9 present the atomic H/C versus O/C ratios for WCPR and DT WCPR samples subjected to different durations of DT at various temperatures.

These diagrams provide valuable insights into the chemical changes occurring in WCPR as a result of DT. The untreated WCPR is positioned at the upper right, indicating higher H/C and O/C ratios. As the temperature increases, the data points move down and to the left, indicating a decrease in both H/C and O/C ratios. The DT_WCPR_300 sample shows the lowest H/C and O/C ratios, indicating significant thermal degradation. The linear regression equation suggests a strong correlation between H/C and O/C ratios. This trend is consistent with the findings of previous studies [14,28].

The plots in Fig. 10a-c illustrate the relationship between FC and VM content in DT WCPR samples. The linear regression lines indicate a strong inverse correlation between FC and VM, with higher torrefaction temperatures leading to higher FC and lower VM content. This trend is consistent across all reaction times. At 60 min, the trend persists with the highest FC content (~41 %) and lowest VM (~52 %) observed for the sample treated at 300 °C. The regression line $y = -0.8933x + 87.78$ with an R^2 value of 0.9899 suggests a strong inverse relationship, similar to the shorter durations but with even higher FC content at elevated temperatures. Higher FC content and lower VM indicate an increase in the energy density of the biochar. Biochar with higher FC is more suitable for applications requiring high energy content, such as solid fuel or as a

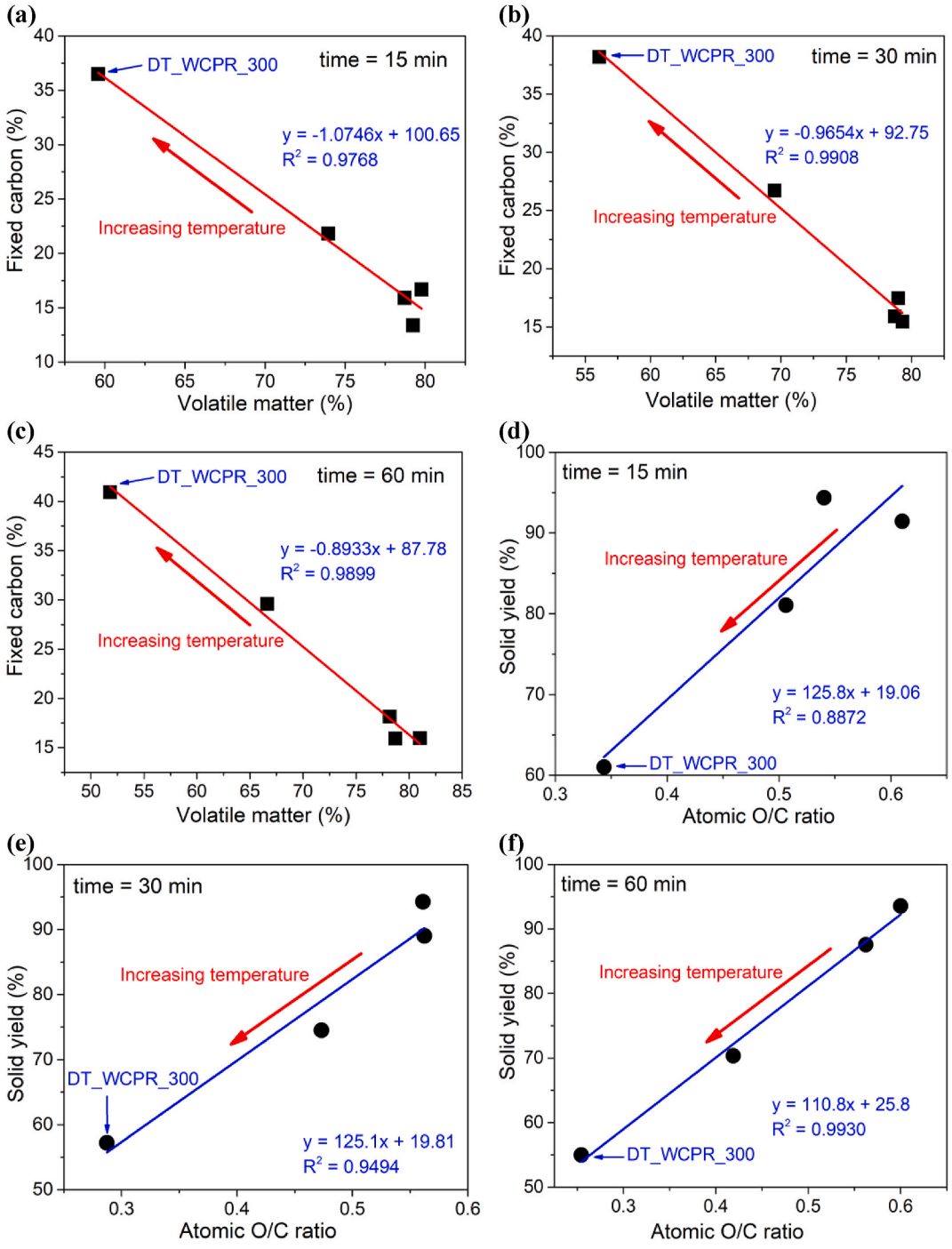

Fig. 10. Fixed carbon versus volatile matter (a–c) and solid yield versus O/C ratio (d–f) for different durations (15–60 min) of DT of WCPR.

reducing agent in metallurgical processes.

The increase in FC content with higher torrefaction temperatures suggests the formation of more stable and less reactive biochar. This stability is advantageous for long-term soil amendment applications, where slow degradation and sustained nutrient release are desired. Moreover, biochars with higher FC and lower VM may exhibit enhanced adsorption properties due to increased surface area and porosity. These properties are beneficial for environmental remediation applications, such as water purification and pollutant adsorption.

The plots in Fig. 10d-f illustrate the relationship between solid yield and atomic O/C, with the linear regression lines highlighting a clear positive correlation between solid yield and atomic O/C ratio, showing that higher torrefaction temperatures lead to lower solid yields and O/C ratios consistently across all reaction durations. At 60 min, the solid yield and atomic O/C ratio show the same trend, with the lowest values observed at 300 °C. The regression line $y = 110.8x + 25.8$ with an R^2 value of 0.9930 indicates an even stronger correlation compared to shorter durations. The prolonged reaction time at higher temperatures results in more complete decomposition and further reduction of the O/C ratio. Lower solid yields and O/C ratios at higher torrefaction temperatures indicate the formation of more stable biochar with lower oxygen content. A lower O/C ratio suggests higher carbon content and lower oxygen content, which can increase the energy density of the biochar. The reduction in the O/C ratio with higher temperatures suggests a decrease in hydrophilic functional groups and an increase in hydrophobicity. This can influence the biochar's adsorption properties and its interactions with water and organic compounds.

The profiles of decarbonization (DC), dehydrogenation (DH), and deoxygenation (DO) for different durations of DT of WCPR are presented in Fig. 11. The data indicate significant variations in the efficiency of these processes over time. As shown in Fig. 11a, after 15 min, there is a noticeable but modest increase in the percentages of DC, DH, and DO across all WCPR temperatures. The highest values are observed for DT_WCPR_300, with DC reaching 21.5 %, DH at around 52 %, and DO close to 57 %. This indicates that even within a short period, the highest temperature (300 °C) significantly enhances the reaction efficiencies, especially for deoxygenation. At 30 min, Fig. 11b illustrates a marked improvement in the reaction processes. Notably, DT_WCPR_300 shows increases with DC of 24 %, DH reaching 56 %, and DO surpassing approximately 65 %. The data for 60 min, depicted in Fig. 11c, further substantiate the trend of increasing efficiency over time. For DT_WCPR_300, DC, DH, and DO achieve their highest levels at about 26 %, 60 %, and 70 %, respectively. These results highlight that prolonged exposure at higher temperatures not only sustains but also enhances the reaction efficiencies.

The enhancement factor, which represents the improvement in key characteristics of the solid product after DT processing, is plotted against carbon enrichment (Fig. S3a–c) and atomic O/C ratio (Fig. S3d–f). The trends observed in these figures provide critical insights into the structural transformations occurring during DT of WCPR. A strong positive linear correlation is evident between the enhancement factor and carbon enrichment across all durations (15–60 min). The regression equations ($R^2 > 0.999$) confirm the robustness of this correlation. This indicates that the increase in carbon content due to DT directly contributes to the enhancement factor. The slope of the linear fits remains relatively stable, with only minor variations, suggesting that the process efficiently

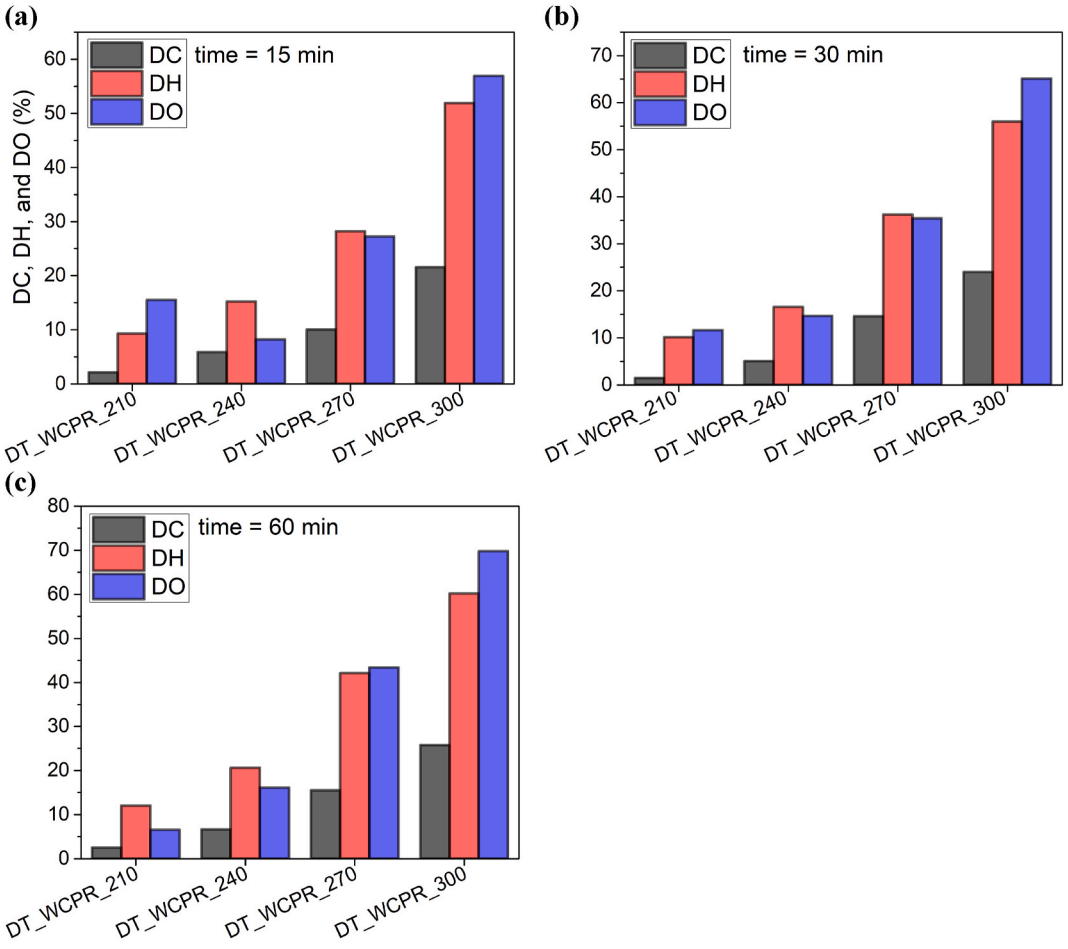

Fig. 11. Profiles of decarbonization (DC), dehydrogenation (DH), and deoxygenation (DO) for different durations of DT of WCPR: 15 min – (a), 30 min – (b), and 60 min – (c).

promotes carbon accumulation irrespective of duration. The arrows indicating "increasing temperature" highlight the expected enhancement in carbon enrichment with higher processing temperatures.

For shorter durations (15 min, Fig. S3a), the enhancement factor increases almost proportionally with carbon enrichment (slope = 0.9801), suggesting rapid initial carbonization. As the duration extends to 30 min (Fig. S3b), the slope remains nearly identical (0.9804), confirming a consistent enhancement rate. However, at 60 min (Fig. S3c), a slightly lower slope (0.9520) suggests that prolonged DT treatment does not further enhance carbon enrichment at the same rate, likely due to a stabilization effect in the conversion process.

A strong negative correlation is observed between the enhancement factor and the atomic O/C ratio, with R^2 values above 0.96 for all cases. The negative slope indicates that as the O/C ratio decreases (signifying deoxygenation), the enhancement factor increases. This trend is consistent with the removal of oxygen-containing functional groups, which is a key indicator of DT efficiency. At the shortest duration (15 min, Fig. S3d), the slope is the steepest (−1.0066), indicating a rapid reduction in the O/C ratio during initial processing. This suggests that the removal of oxygen is particularly efficient in the early stages of DT. As the duration increases to 30 min (Fig. S3e), the slope remains nearly identical (−0.9808), indicating a sustained rate of oxygen removal. However, at 60 min (Fig. S3f), the slope decreases slightly (−0.8936), suggesting that the rate of oxygen loss slows down over time as a result of the stabilization of the chemical composition.

3.8. *Elucidation the reaction pathway for the formation of valuable liquid products in the DT of WCPR*

The DT of WCPR initiates a series of intricate chemical reactions, resulting in the breakdown of cellulose and the formation of various valuable products (Fig. S1). The reaction mechanism of WCPR conversion to LGO and DGP follows an autocatalytic pathway, where thermal degradation generates in situ acidic species such as acetic, levulinic and formic acids. These acids catalyze further depolymerization and dehydration of cellulose, creating a self-sustaining reaction cycle that enhances selectivity toward LGO formation. The presence of these intermediates lowers the activation energy for glycosidic bond cleavage and rearrangement, reinforcing the autocatalytic nature of the process. As the reaction progresses, solid char surfaces may also contribute to additional catalytic effects, further accelerating the transformation of intermediates into target products. Fig. 12 illustrates these transformations, highlighting the major pathways and the yields of main products such as LGO and DGP. The initial step in the mechanism involves the hydrolysis of cellulose into glucose units. This process is facilitated by the addition of water molecules that cleave the glycosidic bonds between the glucose monomers. Once glucose is formed, it can isomerize into fructose, enabling multiple pathways for further chemical transformations. Fructose undergoes dehydration to form 5-HMF, an important intermediate [29]. The dehydration involves the removal of water molecules.

5-HMF itself is a versatile intermediate that can follow multiple reaction pathways. One significant pathway is its further dehydration and rehydration to produce levulinic acid and formic acid. These reactions involve the loss and subsequent addition of water molecules. Alternatively, 5-HMF can undergo condensation reactions to form humins, which are polymeric by-products often considered undesirable due to their recalcitrant nature. In parallel, fructose can also dehydrate to form furfural, a valuable chemical intermediate.

The decomposition of cellulose can lead to the formation of LGA through a dehydration reaction. LGA is a crucial intermediate for further chemical transformations. One significant pathway involves the further

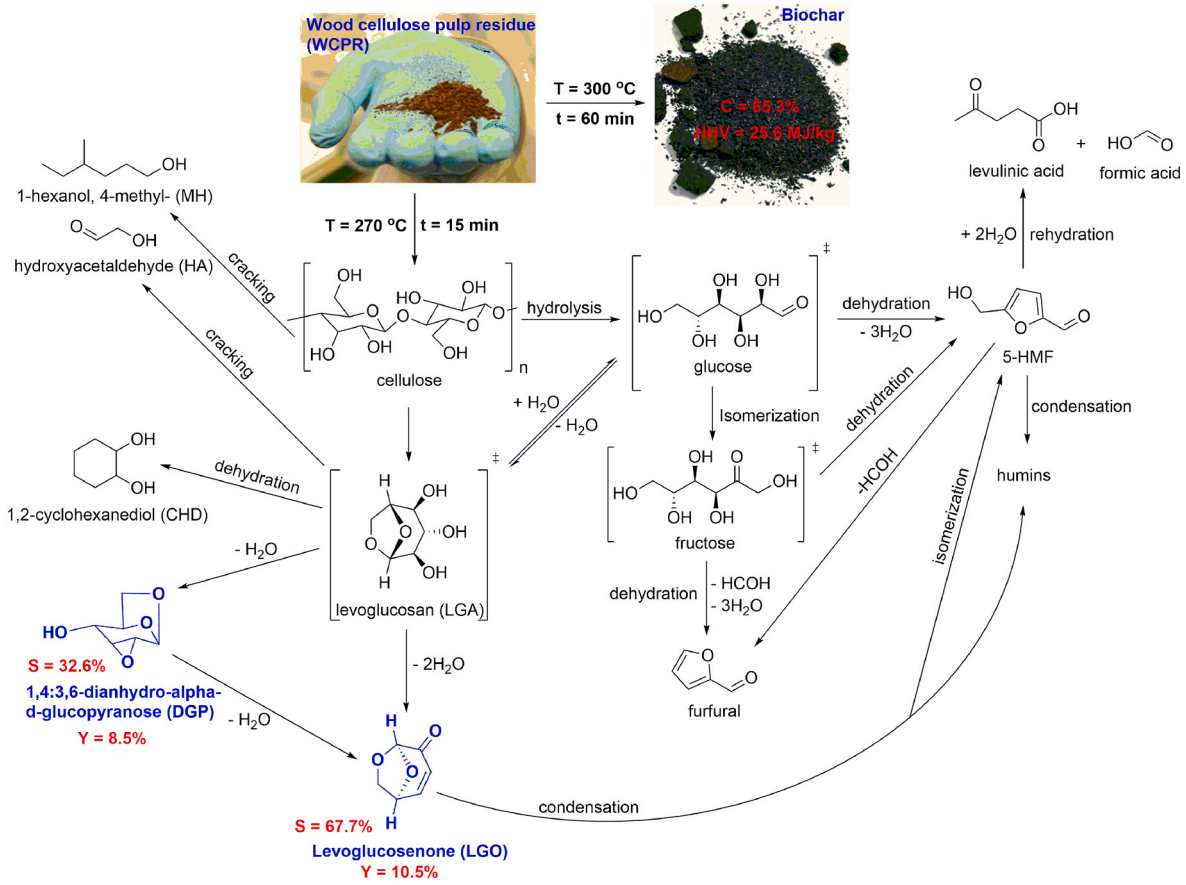

Fig. 12. Reaction pathways of DT of WCPR, leading to biochar and value-added liquid products.

dehydration of LGA to form LGO, achieving an impressive selectivity of 67.7 % and a yield of 10.5 %. Alternatively, LGO can also be indirectly synthesized from DGP [30]. Subsequently, LGO can be isomerized 5-HMF via hydration of the anhydro bridge, followed by ring rearrangement and/or the formation of humins [31]. LGO serves as a valuable chemical intermediate in various industrial applications. Another pathway for LGA involves its dehydration to produce DGP, which has a yield of 8.5 %. Furthermore, LGA can undergo cracking reactions to produce hydroxyacetaldehyde (HA), showcasing its versatility as a precursor for different valuable chemicals. Further cracking of HA can produce 1-hexanol, 4-methyl- (MH), demonstrating the complexity and multiplicity of pathways involved in the thermal treatment of WCPR. Additionally, HA can be converted to 1,2-cyclohexanediol (CHD) through dehydration reaction.

The high selectivity of LGO (67.7 %) and DGP (32.6 %) underscore the efficiency of the DT process in producing valuable chemical intermediates. LGO, in particular, is a key product due to its significant yield and broad industrial applications. These findings highlight the potential of optimizing thermal treatment parameters to maximize the production of desired chemicals from cellulose. In conclusion, the WT of WCPR at 270 °C for 15 min effectively converts cellulose into a variety of valuable chemical products. The detailed mechanism illustrates the complexity of the reaction pathways and emphasizes the importance of conditions such as temperature and time in achieving high yields of specific intermediates. This understanding is crucial for industrial applications aiming to utilize biomass as a sustainable source of chemicals.

The DT conditions reported in this study, moderate temperatures (210–300 °C), short residence times (15–60 min), and N_2 as an inert carrier, are well-aligned with current industrial practices used in biomass thermal pretreatment systems such as fixed bed reactor, rotary kilns (drum) reactor, auger reactor (screw-type reactor), or moving-bed reactor [32]. These technologies already operate under similar temperature and residence time regimes and can be adapted for torrefaction without the need for additional catalysts or solvents, thus simplifying process integration. However, several challenges may arise during scale-up. One key issue is the uniformity of heat transfer in larger-scale reactors, which can influence product selectivity and thermal decomposition profiles. Maintaining a consistent temperature distribution to favor LGO formation without its degradation would require careful reactor design and process control. Additionally, the recovery and separation of volatile value-added compounds like LGO and DGP from the gas stream in a continuous process may require dedicated condensation and purification units, which could increase operational complexity. Despite these challenges, the catalyst-free and solvent-free nature of the process enhances its industrial viability by reducing material costs and simplifying downstream processing.

4. Conclusions

This study demonstrates that dry torrefaction (DT) is an effective low-temperature pretreatment method for converting biomass waste into high-quality biochar and valuable platform chemicals. It was also shown that levoglucosenone (LGO) and 1,4:3,6-dianhydro-α-D-glucopyranose (DGP) can be selectively obtained from wood cellulose pulp residue (WCPR) under solvent- and catalyst-free conditions in N_2 atmosphere. The process is driven by the autocatalytic behavior of WCPR, which generates in situ acidic intermediates that promote selective conversion without the need for external catalysts. The effects of temperature (210–300 °C) and reaction time (15–60 min) on product distribution and biochar properties were systematically investigated. Optimal selectivities for LGO (67.7 %) and DGP (32.6 %) were observed at 270 °C (15 min) and 240 °C (30 min), respectively, while the maximum yields were obtained at 300 °C after 60 min. The resulting biochar exhibited enhanced properties, including a higher heating value of 25.6 MJ/kg, carbon content of 65.3 %, and an energy enhancement factor of 1.33. A comprehensive reaction pathway for cellulose conversion into LGO and DGP was proposed, providing insights into the DT mechanism. These results highlight the potential of catalyst-free biomass valorization strategies that enable simultaneous energy densification and selective production of value-added chemicals, with promising implications for scalable and sustainable process development.

CRediT authorship contribution statement

Andrii Kostyniuk: Writing – review & editing, Writing – original draft, Visualization, Validation, Supervision, Methodology, Investigation, Formal analysis, Data curation, Conceptualization. **Blaž Likozar:** Writing – review & editing, Supervision, Project administration, Funding acquisition, Conceptualization.

Data availability

The data supporting this article have been included as part of the ESI.

Declaration of competing interest

The authors declare that they have no known competing financial interests or personal relationships that could have appeared to influence the work reported in this paper.

Acknowledgements

The authors acknowledge financial support from CARBIOW (Carbon Negative Biofuels from Organic Waste) Research and Innovation Action funded by the European Commission under the Horizon Europe Programme with grant agreement ID: 101084443. The authors are also thankful to Urška Kavčič for N_2 physisorption measurements, Dr. Anže Prašnikar (SEM analysis) and Mr. Edi Kranjc (XRD analysis) and BioTrainValue (BIOmass Valorization via Superheated Steam Torrefaction, Pyrolisis, Gasification Amplified by Multidisciplinary Researchers TRAINining for Multiple Energy and Products' Added VALUEs), with project number: 101086411 (Horizon Europe, Maria Skłodowska-Curie Staff Exchange).

Appendix A. Supplementary data

Supplementary data to this article can be found online at https://doi.org/10.1016/j.renene.2025.123547.

References

[1] W.H. Chen, P.P. Biswas, C. Zhang, E.E. Kwon, J.S. Chang, Achieving carbon credits through biomass torrefaction and hydrothermal carbonization: a review, Renew. Sustain. Energy Rev. 208 (2025) 115056, https://doi.org/10.1016/j.rser.2024.115056.

[2] H.C. Ong, K.L. Yu, W.H. Chen, M.K. Pillejera, X. Bi, K.Q. Tran, A. Pétrissans, M. Pétrissans, Variation of lignocellulosic biomass structure from torrefaction: a critical review, Renew. Sustain. Energy Rev. 152 (2021) 111698, https://doi.org/10.1016/j.rser.2021.111698.

[3] S. Szufa, H. Unyay, Z. Pakowski, P. Piersa, K. Siczek, M. Kabacinski, S. Sobek, K. Moj, B. Likozar, A. Kostyniuk, R. Junga, Batch rolling-bed dryer applicability for drying biomass prior to torrefaction, Renew. Energy 239 (2025) 122106, https://doi.org/10.1016/j.renene.2024.122106.

[4] S. Seraj, R. Azargohar, A.K. Dalai, Dry torrefaction and hydrothermal carbonization of biomass to fuel pellets, Renew. Sustain. Energy Rev. 210 (2025) 115186, https://doi.org/10.1016/j.rser.2024.115186.

[5] L. Leng, L. Yang, J. Chen, Y. Hu, H. Li, H. Li, S. Jiang, H. Peng, X. Yuan, H. Huang, Valorization of the aqueous phase produced from wet and dry thermochemical processing biomass: a review, J. Clean. Prod. 294 (2021) 126238, https://doi.org/10.1016/j.jclepro.2021.126238.

[6] K.A. Abdulyekeen, A.A. Umar, M.F.A. Patah, W.M.A.W. Daud, Torrefaction of biomass: production of enhanced solid biofuel from municipal solid waste and other types of biomass, Renew. Sustain. Energy Rev. 150 (2021) 111436, https://doi.org/10.1016/j.rser.2021.111436.

[7] Q.V. Bach, K.Q. Tran, Ø. Skreiberg, Comparative study on the thermal degradation of dry- and wet-torrefied woods, Appl. Energy 185 (2017) 1051–1058, https://doi.org/10.1016/j.apenergy.2016.01.079.

[8] L. Dai, Y. Wang, Y. Liu, R. Ruan, C. He, Z. Yu, L. Jiang, Z. Zeng, X. Tian, Integrated process of lignocellulosic biomass torrefaction and pyrolysis for upgrading bio-oil production: a state-of-the-art review, Renew. Sustain. Energy Rev. 107 (2019) 20–36, https://doi.org/10.1016/j.rser.2019.02.015.
[9] C. Zhang, Y. Zhan, W.H. Chen, B.Y. Lamba, Y. Zhang, Relative fuel property variation of gas-pressurized and conventional torrefaction for biochar performance assessment, Renew. Energy 235 (2024) 121366, https://doi.org/10.1016/j.renene.2024.121366.
[10] Y. Zhu, Q. Peng, H. Wang, W. Lin, R. Yang, Z. Qi, D. Zhang, L. Ouyang, Predicting the higher heating value of products through solid yield in torrefaction process, Renew. Energy 236 (2024) 121446, https://doi.org/10.1016/j.renene.2024.121446.
[11] I. Itabaiana Junior, M. Avelar Do Nascimento, R.O.M.A. De Souza, A. Dufour, R. Wojcieszak, Levoglucosan: a promising platform molecule? Green Chem. 22 (2020) 5859–5880, https://doi.org/10.1039/d0gc01490g.
[12] F. Cao, T.J. Schwartz, D.J. McClelland, S.H. Krishna, J.A. Dumesic, G.W. Huber, Dehydration of cellulose to levoglucosenone using polar aprotic solvents, Energy Environ. Sci. 8 (2015) 1808–1815, https://doi.org/10.1039/c5ee00353a.
[13] M.B. Comba, Y.H. Tsai, A.M. Sarotti, M.I. Mangione, A.G. Suárez, R.A. Spanevello, Levoglucosenone and its new applications: valorization of cellulose residues, Eur. J. Org Chem. (2018) 590–604, https://doi.org/10.1002/ejoc.201701227.
[14] A. Kostyniuk, B. Likozar, Catalytic wet torrefaction of biomass waste into bio-ethanol, levulinic acid, and high quality solid fuel, Chem. Eng. J. 485 (2024) 149779, https://doi.org/10.1016/j.cej.2024.149779.
[15] A. Kostyniuk, B. Likozar, Wet torrefaction of biomass waste into high quality hydrochar and value-added liquid products using different zeolite catalysts, Renew. Energy 227 (2024) 120509, https://doi.org/10.1016/j.renene.2024.120509.
[16] F. Allais, Total syntheses and production pathways of levoglucosenone, a highly valuable chiral chemical platform for the chemical industry, Curr. Opin. Green Sustain. Chem. 40 (2023) 100744, https://doi.org/10.1016/j.cogsc.2022.100744.
[17] F.P. Bouxin, J.H. Clark, J. Fan, V. Budarin, Combining steam distillation with microwave-assisted pyrolysis to maximise direct production of levoglucosenone from agricultural wastes, Green Chem. 21 (2019) 1282–1291, https://doi.org/10.1039/c8gc02994f.
[18] S. Kudo, N. Goto, J. Sperry, K. Norinaga, J.I. Hayashi, Production of levoglucosenone and dihydrolevoglucosenone by catalytic reforming of volatiles from cellulose pyrolysis using supported ionic liquid phase, ACS Sustain. Chem. Eng. 5 (2017) 1132–1140, https://doi.org/10.1021/acssuschemeng.6b02463.
[19] B. Wang, K. Li, C. bo Zhang, T. Huang, T. peng Wang, Q. Lu, Selective production of levoglucosenone from catalytic pyrolysis of regenerated cellulose from a H3PO4-H2O system, Ind. Crops Prod. 206 (2023), https://doi.org/10.1016/j.indcrop.2023.117594.
[20] O. Oyola-Rivera, J. He, G.W. Huber, J.A. Dumesic, N. Cardona-Martínez, Catalytic conversion of cellulose to levoglucosenone using propylsulfonic acid functionalized SBA-15 and H2SO4 in tetrahydrofuran, Biomass Bioenergy 156 (2022) 106315, https://doi.org/10.1016/j.biombioe.2021.106315.
[21] S. Kudo, X. Huang, S. Asano, J.I. Hayashi, Catalytic strategies for levoglucosenone production by pyrolysis of cellulose and lignocellulosic biomass, Energy Fuels 35 (2021) 9809–9824, https://doi.org/10.1021/acs.energyfuels.1c01062.
[22] A.L. Flourat, L. Pezzana, S. Belgacem, A. Dosso, M. Sangermano, S. Fadlallah, F. Allais, Levoglucosenone to 3D-printed green materials: synthesizing sustainable and tunable monomers for eco-friendly photo-curing, Green Chem. 25 (2023) 7571–7581, https://doi.org/10.1039/d3gc01833d.
[23] F. Xu, J. Luo, L. Jiang, Z. Zhao, Improved production of levoglucosan and levoglucosenone from acid-impregnated cellulose via fast pyrolysis, Cellulose (Lond.) 29 (2022) 1463–1472, https://doi.org/10.1007/s10570-021-04387-4.
[24] B. Hu, A. shuai Cheng, Y. Li, Y. bing Huang, J. Liu, B. Zhang, K. Li, L. Zhao, T. peng Wang, Q. Lu, A sustainable strategy for the production of 1,4:3,6-dianhydro-α-D-glucopyranose through oxalic acid-assisted fast pyrolysis of cellulose, Chem. Eng. J. 436 (2022) 135200, https://doi.org/10.1016/j.cej.2022.135200.
[25] L. Zhao, H. Fu, Y.G. Xia, J. Liu, B. Hu, Z.J. Cheng, X. Luo, D. Yan, J.H. Li, Q. Lu, Coproduction of 1,4:3,6-Dianhydro-α-d-glucopyranose, furfural, and formic acid through oxalic acid-assisted staged fast pyrolysis of cellulose, Energy Fuels 38 (2024) 4302–4311, https://doi.org/10.1021/acs.energyfuels.3c04958.
[26] A. Kostyniuk, B. Likozar, Wet torrefaction of biomass waste into levulinic acid and high-quality hydrochar using H-beta zeolite catalyst, J. Clean. Prod. 449 (2024) 141735, https://doi.org/10.1016/j.jclepro.2024.141735.
[27] A. Kostyniuk, B. Likozar, Wet torrefaction of biomass waste into value-added liquid product (5-HMF) and high quality solid fuel (Hydrochar) in a nitrogen atmosphere, Renew. Energy 226 (2024) 120450, https://doi.org/10.1016/j.renene.2024.120450.
[28] C. Zhang, S.H. Ho, W.H. Chen, Y. Fu, J.S. Chang, X. Bi, Oxidative torrefaction of biomass nutshells: evaluations of energy efficiency as well as biochar transportation and storage, Appl. Energy 235 (2019) 428–441, https://doi.org/10.1016/j.apenergy.2018.10.090.
[29] X. Li, K. Peng, Q. Xia, X. Liu, Y. Wang, Efficient conversion of cellulose into 5-hydroxymethylfurfural over niobia/carbon composites, Chem. Eng. J. 332 (2018) 528–536, https://doi.org/10.1016/j.cej.2017.06.105.
[30] A. Doroshenko, I. Pylypenko, K. Heaton, S. Cowling, J. Clark, V. Budarin, Selective microwave-assisted pyrolysis of cellulose towards levoglucosenone with clay catalysts, ChemSusChem 12 (2019) 5224–5227, https://doi.org/10.1002/cssc.201903026.
[31] S.H. Krishna, T.W. Walker, J.A. Dumesic, G.W. Huber, Kinetics of levoglucosenone isomerization, ChemSusChem 10 (2017) 129–138, https://doi.org/10.1002/cssc.201601308.
[32] W.H. Chen, B.J. Lin, Y.Y. Lin, Y.S. Chu, A.T. Ubando, P.L. Show, H.C. Ong, J. S. Chang, S.H. Ho, A.B. Culaba, A. Pétrissans, M. Pétrissans, Progress in biomass torrefaction: principles, applications and challenges, Prog. Energy Combust. Sci. 82 (2021) 100887, https://doi.org/10.1016/j.pecs.2020.100887.